







RESEARCH ARTICLE | FEBRUARY 17 2023

Probing power laws in multifrequency AFM

Sergio Santos ; Karim Gadelrab ; Tuza Olukan ; Josep Font ; Victor Barcons ; Matteo Chiesa 

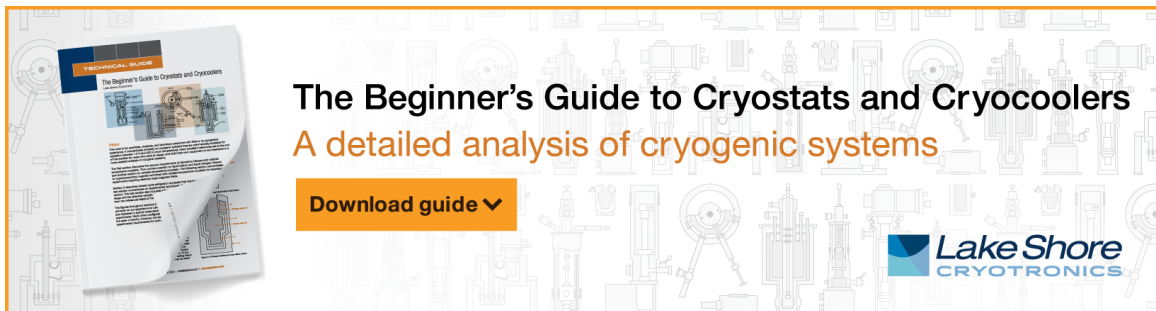


Appl. Phys. Lett. 122, 071603 (2023)

<https://doi.org/10.1063/5.0141741>




CrossMark



The Beginner's Guide to Cryostats and Cryocoolers
A detailed analysis of cryogenic systems

[Download guide](#)



Probing power laws in multifrequency AFM

Cite as: Appl. Phys. Lett. **122**, 071603 (2023); doi: 10.1063/5.0141741

Submitted: 8 January 2023 · Accepted: 26 January 2023 ·

Published Online: 17 February 2023





View Online



Export Citation



CrossMark

Sergio Santos,^{1,a)}  Karim Gadelrab,²  Tuza Olukan,¹  Josep Font,³  Victor Barcons,³ 
and Matteo Chiesa^{1,4,a)} 

AFFILIATIONS

¹Department of Physics and Technology, UiT-the Arctic University of Norway, 9037 Tromsø, Norway

²Department of Materials Science and Engineering, Massachusetts Institute of Technology, Cambridge, Massachusetts 02139, USA

³Departament d'Enginyeria Minera, Industrial i TIC, UPC BarcelonaTech, 08242 Manresa, Spain

⁴Laboratory for Energy and NanoScience (LENS), Khalifa University of Science and Technology, Masdar Institute Campus, 127788 Abu Dhabi, United Arab Emirates

^{a)} Authors to whom correspondence should be addressed: ssantos78h@gmail.com and matteo.chiesa@ku.ac.ae

ABSTRACT

Quantification of conservative forces in multifrequency atomic force microscopy requires solving the general equations of the theory expressed in terms of the virials of interaction. Power law expressions are commonly utilized when dealing with electrostatic, ferroelectric, magnetic, or long range (van der Waals) forces. Here, we discuss long range forces modeled in terms of power laws (n), where the exponent n covers the range $n = 2-5$, and employ the multifrequency theory to explore the relevant parameter space. Numerical integration of the equations of motion suggest that only a narrow range of operational parameters are available when imaging where the approximations are valid. Albeit these conditions exist, and the corresponding errors can be as low as 10% throughout for all exponents explored.

© 2023 Author(s). All article content, except where otherwise noted, is licensed under a Creative Commons Attribution (CC BY) license (<http://creativecommons.org/licenses/by/4.0/>). <https://doi.org/10.1063/5.0141741>

The virial of interaction¹⁻⁴ and the energy dissipation expressions^{5,6} form the basis of the theory of dynamic atomic force microscopy (AFM),^{7,8} and more generally, of multifrequency atomic force microscopy⁹ (AFM). The virial of interaction, also known in the field as virial, is known to control the frequency shift. The theory of frequency modulation (FM) AFM uses the virial expression to establish the relationship between the conservative tip sample force and the frequency shift.^{4,10} In the absence of dissipative interactions, the relationship between the amplitude decay and the force is also known to be controlled by the virial¹ in amplitude modulation (AM) AFM. Expressions for the virial can be written in terms of experimental observables in both FM and AM AFM, i.e., in terms of frequency shift and amplitude in FM and in terms of amplitude and phase shift in AM correspondingly. More importantly, analytical expressions can be derived for the virial, as a time integral of the displacement weighted tip sample force, when force models are proposed. Such models can contain material properties, such as materials stiffness,¹¹⁻¹³ adhesion,¹⁴ viscoelasticity,^{12,15} or the Hamaker,^{16,17} a parameter employed to quantify the London dispersion force as a fundamental part of van der Waals forces. Simultaneously solving these expressions, and provided there are as many equations as unknowns, leads to a quantitative and rapid method to extract material properties^{12-14,16-20} with nanometric resolution in multifrequency AFM. In the long range, i.e., for the forces

acting before mechanical contact, it is typical to consider the ubiquitous van der Waals (vdW) interaction where an inverse square law is predicted to follow for the interaction between a sphere, i.e., an AFM tip modeled as a sphere of radius R , and a surface. The inverse square law is predicted for these systems when considering the original Hamaker²¹ and Lifshitz²² theories. We showed, however, that experimental force profiles might not align with inverse power laws in air.²³ In addition, there are other phenomena of interest to the field involving power laws, such as electrostatic,²⁴⁻²⁷ ferroelectric,^{28,29} and magnetic³⁰⁻³³ phenomena.

Here, we focus on long range forces modeled in terms of power laws and employ the multifrequency theory to discuss these forces and the relevant parameter space to minimize errors while imaging. To this end, we solve the governing integral equations analytically and via numerical integration for powers 2-5.

The standard theory of multifrequency AFM is based on several assumptions.⁹ First, the dynamics of the cantilever-tip system are described in terms of the beam theory.³⁴ Second, the system is reduced to a set of M ($m = 1 \dots M$, where m stands for eigenmode modes) second order differential equations. The governing equations of motion in multifrequency AFM are written in terms of these M equations. Each equation is identical to the standard differential equations found in the linear theory for the driven oscillator,^{35,36} albeit, a nonlinear

term, i.e., the tip-sample force F_{ts} , and multiple drives also contribute. Here, we take $M=2$ and describe the system by the first two eigenmodes,

$$m\ddot{z}_1 = -k_1 z_1 - \frac{m\omega_{01}}{Q_1} \dot{z}_1 + F_{01} \cos \omega_1 t + F_{02} \cos \omega_2 t + F_{ts}(z_1 + z_2), \tag{1}$$

$$m\ddot{z}_2 = -k_2 z_2 - \frac{m\omega_{02}}{Q_2} \dot{z}_2 + F_{01} \cos \omega_1 t + F_{02} \cos \omega_2 t + F_{ts}(z_1 + z_2), \tag{2}$$

where the subscripts 1 and 2 stand for modes 1 and 2, respectively. The subscripts 01 and 02 stand for natural frequency of modes 1 and 2, respectively. The drives are F_{01} and F_{02} for modes 1 and 2, respectively. The terms $z_1(t)$ and $z_2(t)$ are the modal projections of the tip trajectory, m is the effective mass, Q_i are the Q factors, k_i are the effective spring constants, ω_{0i} are the angular natural frequencies, and ω_i are the angular drive frequencies. Typically $\omega_{0i} \approx \omega_i$. The solution to the above-mentioned equations is⁹

$$z(t) = z_1(t) + z_2(t) + O(\varepsilon), \tag{3}$$

$$\approx A_1 \cos(\omega_1 t - \phi_1) + A_2 \cos(\omega_2 t - \phi_2),$$

where $O(\varepsilon)$ is the term carrying the contributions of higher harmonics and higher modes, A_i are the amplitudes, and ϕ_i are the phase shifts. The power laws under investigation here take the following form:^{23,37,38}

$$F_{ts}(\alpha, n) = -\frac{\alpha}{d^n} \quad d > a_0, \tag{4}$$

where α dictates the magnitude of the phenomena, d is the instantaneous tip-sample distance, the power n dictates the profile of the force, and a_0 is an intermolecular distance that implies that matter interpenetration cannot occur.^{22,39} The higher the power n the faster the force decays. In the limit where n is very large F_{ts} is significant only where $d \approx a_0$. The Hamaker theory²¹ provides a way to write α in terms of physically meaningful parameters for $n = 2$, i.e., the London dispersion forces. Then,

$$\alpha = \frac{RH}{6}, \tag{5}$$

where R is the tip radius modeled as a sphere and H is the Hamaker coefficient the units of which are Joules. Empirical values for H can be found in the literature²² and are shown to depend on the size of the atoms, the packing, and electronegativity. Furthermore, according to the Lifshitz theory, H depends on the dielectric properties of the interacting materials and the medium, implying that dielectric properties, the size of the atoms, packing, and electronegativity are related. When $d = a_0$, the force in (4) must coincide with the adhesion force⁴⁰ F_{AD} ,

$$F_{AD} = -\frac{\alpha}{a_0^n} \equiv -4\pi R\gamma, \tag{6}$$

where γ is the surface energy. Equation (6) allows us to set a value for A_0 , R , and γ and establish the value of α independently of n . The virial of interaction V_i includes the conservative^{1,2} (or even⁴¹) forces which are the ones of interest here in terms of (4). The virial expressions V_i can be found in multifrequency AFM by combining Eqs. (1)–(3),

$$V_i = \langle F_{ts} z_i \rangle_i = \frac{1}{T} \int_0^T F_{ts} z_i dt, \tag{7}$$

where T is the fundamental period $T = 2\pi/\omega_1$. The two alternative ways to find the virials follow. First, the expression in (7) can be found generically in terms of experimental observables by combining (1)–(3) and (7). The solutions are ($\omega_{0i} \approx \omega_i$),

$$V_i = -\frac{1}{2} F_{0i} A_i \cos \phi_i \quad \text{where} \quad F_{0i} = \frac{k_i A_{0i}}{Q_i} \quad \text{at} \quad \omega_i = \omega_{0i}. \tag{8}$$

The virials V_i can, thus, be extracted empirically in AM AFM by calibrating k_i , Q_i , and the “free” amplitudes A_{0i} and inserting the observables A_i and ϕ_i into (8). In 2001, San Paulo and García showed that (8) is a very good approximation to the virial.¹ In FM AFM, the experimental observable is the (relative) frequency shift $\Delta\omega_{0i}/\omega_{0i}$. The virial can be rewritten as^{2,42,43}

$$V_i \approx -k_i A_i^2 \frac{\Delta\omega_{0i}}{\omega_{0i}}. \tag{9}$$

Expressions (8) and (9) show that the expressions in AM and FM can be combined to indirectly find observables.

Second, inserting (3) and (4) into (7) provides a means to express V_i in terms of material properties. We note that Amo discussed similar solutions³⁷ in his PhD thesis in 2019. For the first virial, and provided $A_1 \gg A_2$, the approximation $d_m \approx z_c - A_1$ holds (z_c is the cantilever separation). Then, the contributions of the second mode can be neglected. For powers $n = 2-5$, we find

$$V_1(n=2) \approx \frac{\alpha}{A_1} \left[\left(\frac{z_c}{A_1} \right)^2 - 1 \right]^{-3/2},$$

$$V_1(n=3) \approx \frac{3\alpha}{A_1^2} \left[\frac{z_c}{A_1} \right] \left[\left(\frac{z_c}{A_1} \right)^2 - 1 \right]^{-5/2}, \tag{10}$$

$$V_1(n=4) \approx \frac{\alpha}{2A_1^3} \left[4 \left(\frac{z_c}{A_1} \right)^2 + 1 \right] \left[\left(\frac{z_c}{A_1} \right)^2 - 1 \right]^{-7/2},$$

$$V_1(n=5) \approx \frac{\alpha}{8A_1^4} \left[20 \left(\frac{z_c}{A_1} \right)^3 + 15 \left(\frac{z_c}{A_1} \right) \right] \left[\left(\frac{z_c}{A_1} \right)^2 - 1 \right]^{-9/2}.$$

Finding the virial for the second mode, and provided $A_1 \gg A_2$, requires making several assumptions. In 2009, Kawai *et al.* proposed⁴⁴ that the averaged frequency shift of the second mode over the fundamental period could be approximated to

$$\frac{\Delta\omega_{02}}{\omega_{02}} \approx -\frac{1}{2k_2 T} \oint \frac{\partial F_{ts}}{\partial d} dt. \tag{11}$$

Combining (9) and (11)

$$V_i \approx \frac{A_i^2}{2T} \oint \frac{\partial F_{ts}}{\partial d} dt. \tag{12}$$

The derivative in the integral in (12) can be obtained by deriving (4) in terms of d . Inserting that derivative into (12) and combining with (3) while also using the approximation $d_m \approx z_c - A_1$,

$$\begin{aligned}
 V_2(n=2) &\approx \alpha \left[\frac{A_2}{A_1} \right]^2 \frac{1}{A_1} \left[\left(\frac{z_c}{A_1} \right)^2 + \frac{1}{2} \right] \left[\left(\frac{z_c}{A_1} \right)^2 - 1 \right]^{-5/2}, \\
 V_2(n=3) &\approx \frac{\alpha}{2} \left[\frac{A_2}{A_1} \right]^2 \frac{1}{A_1^2} \left[2 \left(\frac{z_c}{A_1} \right)^3 + 3 \left(\frac{z_c}{A_1} \right) \right] \\
 &\quad \times \left[\left(\frac{z_c}{A_1} \right)^2 - 1 \right]^{-7/2}, \\
 V_2(n=4) &\approx \frac{\alpha}{8} \left[\frac{A_2}{A_1} \right]^2 \frac{1}{A_1^3} \left[8 \left(\frac{z_c}{A_1} \right)^4 + 24 \left(\frac{z_c}{A_1} \right)^2 + 3 \right] \\
 &\quad \times \left[\left(\frac{z_c}{A_1} \right)^2 - 1 \right]^{-9/2}, \\
 V_2(n=5) &\approx \frac{\alpha}{8} \left[\frac{A_2}{A_1} \right]^2 \frac{1}{A_1^4} \left[8 \left(\frac{z_c}{A_1} \right)^5 + 40 \left(\frac{z_c}{A_1} \right)^3 + 15 \left(\frac{z_c}{A_1} \right) \right] \\
 &\quad \times \left[\left(\frac{z_c}{A_1} \right)^2 - 1 \right]^{-11/2}.
 \end{aligned} \tag{13}$$

Constraints: Aksoy and Atalar⁴² later showed that the derivation of (11) comes with upper and lower bound constraints for A_2 as follows:

$$\pi^2 A_1 \frac{\omega_{01}^2}{\omega_{02}} T_c \ll A_2 \ll 2 \left\| \frac{F_{is}''(z_1(t))}{F_{is}'''(z_1(t))} \right\|. \tag{14}$$

The term on the left is based on the small angle approximation for the sine function and is parameterized physically by T_c , i.e., the time during an oscillation cycle for which the interaction is significant. T_c is small when F_{is} is large enough to significantly affect the dynamics only for a small fraction of the fundamental period T . Furthermore, T_c must be small to allow for larger values of A_2 to be valid. In principle, T_c can be forced to be small by making A_1 large, but there is a problem when making A_1 large. From the left of (14), we see that A_1 cannot be made arbitrarily large for a given A_2 . The upper bound on the right comes from a power series expansion where higher order derivatives can be neglected. The upper bound on the right of (14) further forces the values of A_2 to be small in relation to the interaction parameterized by the second and third derivatives. Finally, the approximation $d_m \approx z_c - A_1$ employed to derive both virials 1 and 2 implies that d_m must be controlled by A_1 and this happens only when $A_1 \gg A_2$. This further constrains the lower bound of (14). With all these consideration, we start by checking the approximations of V_1 and V_2 in (10) and (13) for $n=2$ as a function of A_{01} and A_{02} by numerical integration of the equations of motion in (1) and (2). In Figs. 1(a)–1(c), $A_{01} = 2$ and $A_{02} = 0.2$ nm and in Figs. 1(a)–1(c), $A_{01} = 5$ and $A_{02} = 0.1$ nm. The parameters used in the simulation are shown in the figure caption. The values for V_i computed directly from the numerical integration are shown in blue squares and the analytic predictions are shown in orange circles. The values are normalized as indicated with the asterisk. The bottom panels also show the approximation for V_1 where¹

$$V_1 \approx V_{Z_0} \approx -A_1 \langle F_{is} \rangle = -A_1 k_1 z_0. \tag{15}$$

The approximation in (15), first derived by San Paulo and García in 2001, assumes that $T_c/T \ll 1$ where T is the fundamental period. The

expression in (15) allows checking whether the condition on the left of (14) is satisfied in terms of T_c . The analysis of (14) in Figs. 2–4 requires discussing a further detail. A_2 and A_1 will be assumed to be directly controlled by A_{01} and A_{02} . Thus, the figures will be discussed by referring to these “free” values rather than to A_1 and A_2 in (14), but the results are otherwise relevant in multifrequency AFM. We use the free amplitudes as the variables because these can be easily set by users in amplitude modulation AFM. The next figures and discussion aim to show that users should use values where the ratio A_{01}/A_{02} is approximately 10. The set point of amplitude 1, A_1 , is also controlled by the user. In this respect, we will also show that experiments should be conducted for $A_1/A_{01} > 0.8$.

Several results are worth mentioning for Fig. 1. First, the errors in V_1 are relatively small, i.e., $\sim 10\%$, since $A_{01} \gg A_{02}$ for both examples. The error in the second virial, V_2 , also stays “small” when $A_{01} = 2$ nm and $A_{02} = 0.2$ nm [Fig. 1(b)]. Yet, increasing the ratio A_{01}/A_{02} by a factor of 5 results in larger errors, i.e., $\sim 20\%$ – 40% , for V_2 [Fig. 1(e)]. The approximation in (15) is better for V_2 when the ratio A_{01} increases as seen by comparing Figs. 1(c) and 1(f). Figures 2 and 3 illustrate what happens when varying A_{02} and A_{01} , respectively, for $n=2$ only as before. The normalized errors are plotted directly in these figures by subtracting the values of the normalized numerical results (num) from the analytic results (analytic) as given in Eqs. (10) and (13) for V_1 and V_2 , respectively, for the different powers n . We note that V_1 peaks at $A_1/A_{01} \sim 0.5$ – 0.8 since in the extremes either F_{is} or z_i are close to zero implying that the integral in (7) is close to zero.

In Fig. 2, $A_{01} = 2$ and $A_{02} = 0.05$ – 2 nm. For V_1 [Fig. 2(a)], the analytic expressions do well only where the ratio A_{01}/A_{02} is large, i.e., see crosses and circles, where $A_{02} = 0.2$ nm and 50 pm, respectively. This is consistent with (14) and $d_m \approx z_c - A_1$. For V_2 [Fig. 2(b)], the best results are obtained where A_{02} is neither too small nor too large relative to A_{01} , i.e., see crosses where $A_{02} = 0.2$ nm, also in agreement with (14). In particular, the best results occur where $A_{01}/A_{02} \approx 0.1$. The errors in approximation (15) are very large throughout [Fig. 2(c)] implying that T_c is “large.” This means that, according to (14), the errors in V_2 are controlled by the ratio A_{01}/A_{02} alone and T_c constraints A_{02} to be “large,” compromising the range of A_{02} that make the analytic solutions valid.

In Fig. 3, $A_{02} = 0.1$ and $A_{01} = 0.2$ – 5 nm. For V_1 [Fig. 3(a)], the analytic expressions do better where the ratio A_{01}/A_{02} is large as before, i.e., see black circles where $A_{01} = 0.2$ nm for very larger errors. Again, this is consistent with what has been said regarding (14) and $d_m \approx z_c - A_1$. For V_2 [Fig. 3(b)], the best results are obtained where A_{01} is small enough relative to A_{02} . The combination of these two results, and in order to optimize results, the smaller [circles in Fig. 3(a)] and larger [squares in Fig. 3(b)] ratios must be disregarded. Again optima are found for ratios $A_{01}/A_{02} \sim 0.1$ – 0.2 , i.e., triangles and crosses in Figs. 3(a) and 3(b). The errors in the approximation (15) are largest for the smaller values of A_{01} [Fig. 3(c)]. For larger A_{01} values, i.e., 2 (triangles) and 5 nm (squares), T_c is “small.” Thus, according to (14), the errors in V_2 are controlled by the ratio A_{01}/A_{02} and the upper bound of (14), i.e., the higher derivatives.

For the last figure, Fig. 4, we select “an optimum” and a “non-optimum” set of parameters as found from the analysis in Figs. 1–3 and in agreement with (14). In particular, $A_{01} = 2$ and $A_{02} = 0.2$ nm for the figures on the left panel and $A_{01} = 5$ and $A_{02} = 0.2$ nm for the figures on the right panel. Again, the errors are shown for normalized

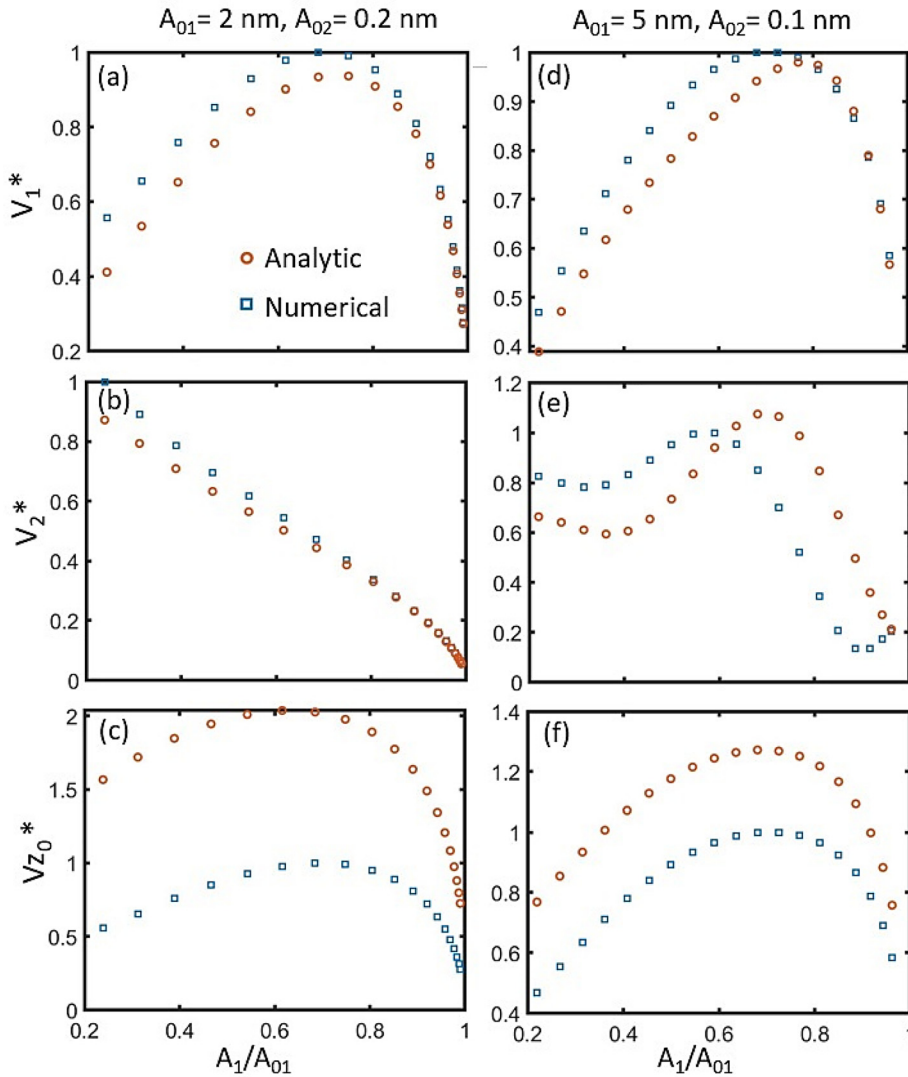


FIG. 1. Numerical results showing the behavior of (a) and (d) virial 1 (V_1), (b) and (e) virial 2 (V_2), and (c) and (f) the approximation V_{Z_0} in (15). The values are normalized as indicated by the asterisks. The results are shown where (a)–(c) $A_{01} = 2$ and $A_{02} = 0.2$ nm and (d)–(f) $A_{01} = 5$ and $A_{02} = 0.1$ nm. The results obtained numerically from the definition of (7) are shown in blue squares and the analytic predictions from (10), (13), and (15) are shown in orange circles. The results have been obtained by assuming $n = 2$ in (4). The numerical integration was carried out by setting $k_1 = 2$ N/m, $k_2 = 80$ N/m, $f_{01} = 70$ kHz, $f_{02} = 420$ kHz, $Q_1 = 100$, and $Q_2 = 600$ for the cantilever parameters. For the physical parameters, the values are $R = 20$ nm, $a_0 = 0.165$ nm, and $\gamma = 20$ mJ m $^{-2}$. The values used for normalization are V_1 (max) = 20 and V_2 (max) = 1.3 zeptojoules.

values of V_1 [Figs. 4(a) and 4(d)], V_2 [Figs. 4(b) and 4(e)], and V_{Z_0} [Figs. 4(c) and 4(f)]. The results here are shown for powers $n = 2$ (squares), 3 (circles), and 4 (crosses). The results for $n = 5$ are not shown because the errors increase exponentially. In terms of the optimum conditions, i.e., left panels, the errors are reasonable, i.e., $\sim 10\%$ – 20% , for both V_1 and V_2 for all powers n (except $n = 4$) provided $A_1/A_{01} > 0.7$ – 0.8 . In AM AFM, this translates into “soft tapping” in the attractive regime and is consistent with standard imaging conditions. For smaller A_1/A_{01} ratios, the errors are very large, and assumptions break down, and more so, as the power n increases. See as an example the crosses in Figs. 4(a)–4(e). One explanation is that increasing n implies increasing the relative weight of higher order derivatives [see the upper bound limit in (14)], i.e., the force is too steep. The situation is worse when the ratio A_{01}/A_{02} increases (see panels on the right in Fig. 4). Finally, the approximation in (15) improves with increasing n . Compare crosses and circles in Figs. 4(c) and 4(f) with

squares. This is consistent with increasing steepness and, thus, with decreasing values of T_C . The shaded areas (gray) show the “high” set-points of operation where the ratio $A_{01}/A_{02} \approx 10$ and set point $A_1/A_{01} \approx 0.8$ lead to smallest errors. Finally, we also note that when $A_{01}/A_{02} \gg 10$ [Figs. 4(d)–4(f)] and the ratio A_1/A_{01} leads to conditions where $A_1/A_{02} < 10$, the errors in both V_1 and V_2 are optimum.

In conclusion, we have derived analytic expressions for the virials of interaction in multifrequency AFM for powers ranging from 2 to 5. Such models are employed when modeling phenomena involving attractive surface forces. When the power is 2, the expressions agree with the Hamaker and Lifshitz theories, i.e., the force is inversely proportional to the square of the tip-sample distance. Comparisons with the numerical integration of the equations of motion suggest that a narrow range of operational parameters are available when imaging where the approximations are valid. Albeit these conditions exist, and the corresponding errors can be as small as 10% throughout for all

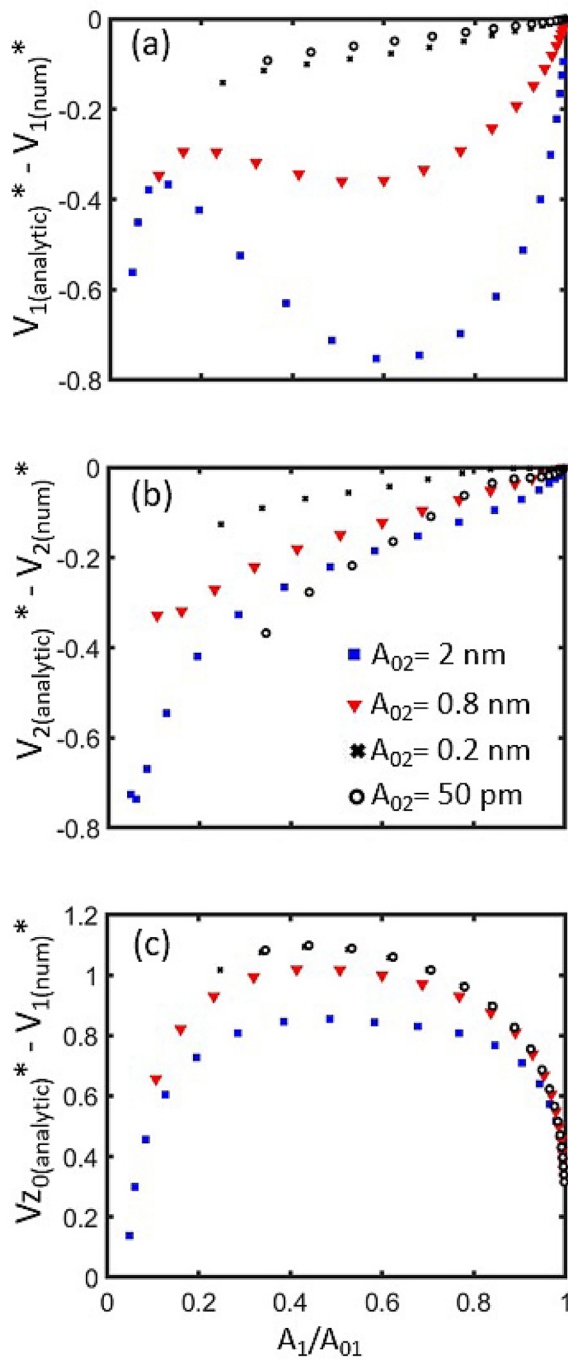


FIG. 2. Numerical results showing the behavior of (a) virial 1 (V_1), (b) virial 2 (V_2), and (c) the approximation V_{Z_0} in (15). The values are normalized as indicated by the asterisks and only errors are shown. The results are shown for $A_{01} = 2$ nm and $A_{02} = 50$ pm (black circles), 0.2 nm (crosses), 0.8 nm (red triangles), and 2 nm (blue squares). The results have been obtained by assuming $n = 2$ in (4). The values used for normalization are $A_{02} = 50$ pm— V_1 (max) = 20 and V_2 (max) = 0.1 zeptojoules; $A_{02} = 0.2$ nm— V_1 (max) = 20 and V_2 (max) = 1.3 zeptojoules; $A_{02} = 0.8$ nm— V_1 (max) = 20 and V_2 (max) = 21 zeptojoules; and $A_{02} = 2$ nm— V_1 (max) = 20 and V_2 (max) = 133 zeptojoules. Other parameters as in Fig. 1.

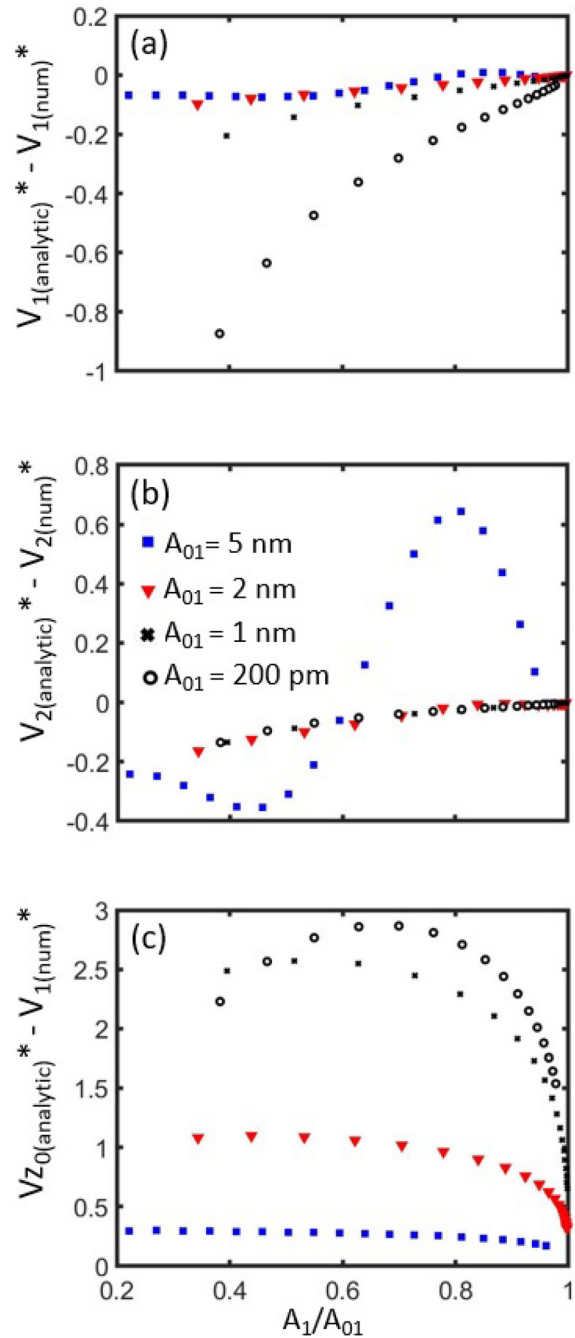


FIG. 3. Numerical results showing the behavior of (a) virial 1 (V_1), (b) virial 2 (V_2), and (c) the approximation V_{Z_0} in (15). The values are normalized as indicated by the asterisks and only errors are shown. The results are shown for $A_{02} = 100$ and $A_{01} = 200$ pm (black circles), 1 nm (crosses), 2 nm (red triangles), and 5 nm (blue squares). The results have been obtained by assuming $n = 2$ in (4). The values used for normalization are $A_{01} = 200$ pm— V_1 (max) = 1 and V_2 (max) = 0.2 zeptojoules; $A_{01} = 1$ nm— V_1 (max) = 5.3 and V_2 (max) = 0.2 zeptojoules; $A_{01} = 2$ nm— V_1 (max) = 20 and V_2 (max) = 0.3 zeptojoules; and $A_{01} = 5$ nm— V_1 (max) = 123 and V_2 (max) = 0.6 zeptojoules. Other parameters as in Fig. 2.

18 July 2023 06:16:32

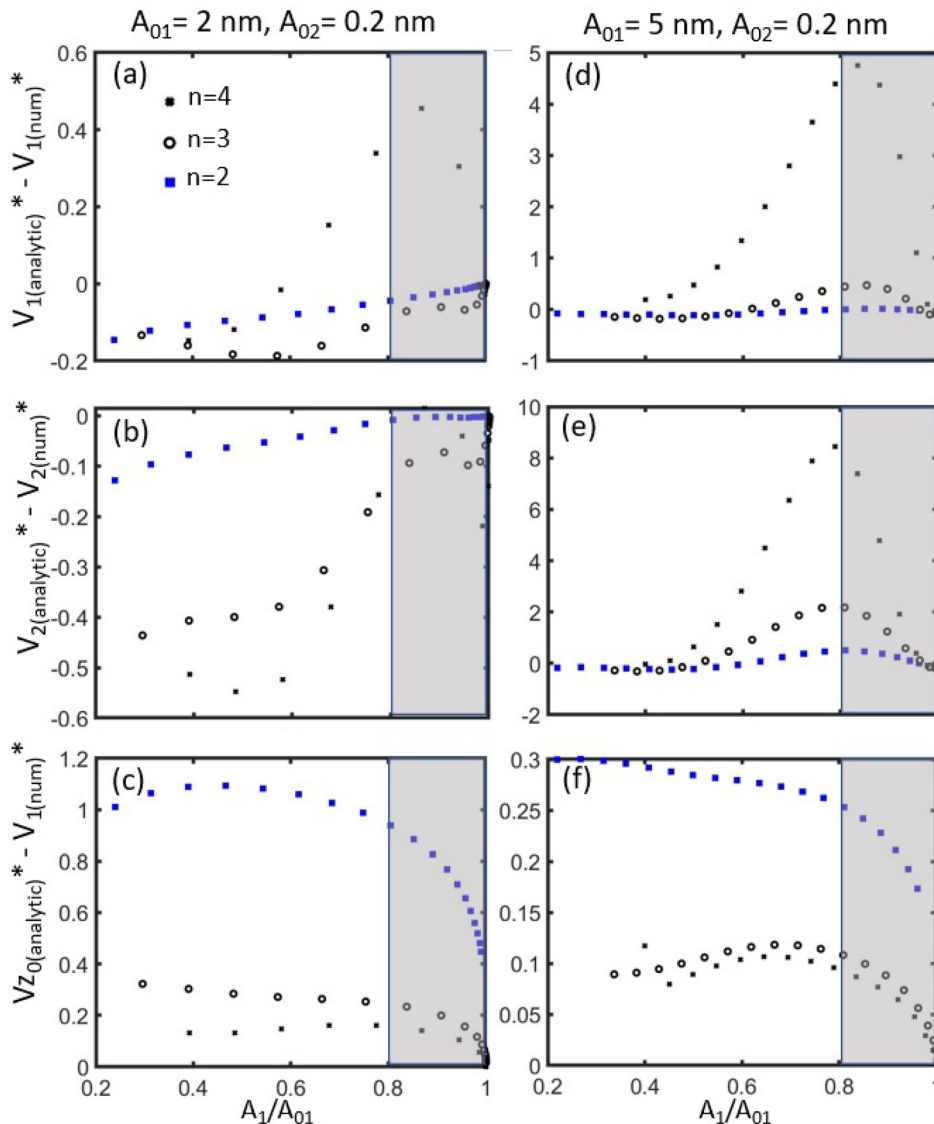


FIG. 4. Numerical results showing the behavior of (a) and (d) virial 1 (V_1), (b) and (e) virial 2 (V_2), and (c) and (f) the approximation V_{Z_0} in (15). The values are normalized as indicated by the asterisks and only errors are shown. The results are shown for $A_{01} = 2$ and $A_{02} = 0.2$ nm on the panels and for $A_{01} = 5$ and $A_{02} = 0.2$ nm on the right panels. The markers stand for the powers $n = 2$ (blue squares), $n = 3$ (black circles), and $n = 4$ (crosses) in (4). Other parameters as in Fig. 3. The shaded areas (gray) show the “high” set-points of operation where the ratio $A_{01}/A_{02} \approx 10$ and set point $A_1/A_{01} \approx 0.8$ lead to smallest errors.

powers explored, i.e., normalized error being 0.1 or less in Figs. 2–4 except for V_1 and $n = 4$ [Fig. 4(a)], where errors are slightly larger for high set-points. Roughly, optima is obtained when the free amplitude of the first mode ~ 1 nm and the free amplitude of the second mode is about 10% the value of the first amplitude for sufficiently high but standard set points, i.e., $A_1/A_{01} > 0.8$.

AUTHOR DECLARATIONS

Conflict of Interest

The authors have no conflicts to disclose.

Author Contributions

Sergio Santos and Karim Gadelrab contributed equally to this paper.

Sergio Santos: Conceptualization (lead); Data curation (equal); Formal analysis (equal); Investigation (equal); Methodology (equal); Validation (equal); Visualization (equal); Writing – original draft (lead); Writing – review & editing (equal). **Karim Gadelrab:** Conceptualization (equal); Formal analysis (equal); Investigation (equal); Methodology (equal); Validation (equal); Visualization (equal); Writing – original draft (supporting); Writing – review & editing (equal). **Tuza Adeyemi Olukan:** Conceptualization (supporting); Formal analysis (supporting); Investigation (equal); Methodology (supporting); Writing – original draft (supporting); Writing – review & editing (equal). **Josep Font:** Conceptualization (equal); Formal analysis (equal); Investigation (supporting); Methodology (equal); Validation (supporting); Visualization (supporting); Writing – review & editing (supporting). **Victor Barcons:** Conceptualization (equal); Data curation (equal); Formal analysis (equal); Investigation

(equal); Methodology (equal); Validation (supporting); Visualization (supporting); Writing – original draft (supporting); Writing – review & editing (supporting). **Matteo Chiesa:** Conceptualization (equal); Data curation (supporting); Formal analysis (equal); Funding acquisition (lead); Investigation (equal); Methodology (supporting); Project administration (lead); Resources (lead); Supervision (lead); Validation (supporting); Visualization (supporting); Writing – original draft (supporting); Writing – review & editing (supporting).

DATA AVAILABILITY

The data that support the findings of this study are available from the corresponding authors upon reasonable request.

REFERENCES

- ¹Á. S. Paulo and R. García, *Phys. Rev. B* **64**(19), 193411 (2001).
- ²F. J. Giessibl, *Phys. Rev. B* **56**(24), 16010 (1997).
- ³J. E. Sader and S. P. Jarvis, *Phys. Rev. B* **70**(1), 012303 (2004).
- ⁴J. E. Sader, T. Uchihashi, M. J. Higgins, A. Farrell, Y. Nakayama, and S. P. Jarvis, *Nanotechnology* **16**(3), S94 (2005).
- ⁵J. P. Cleveland, B. Anczykowski, A. E. Schmid, and V. B. Elings, *Appl. Phys. Lett.* **72**(20), 2613–2615 (1998).
- ⁶J. Tamayo and R. García, *Appl. Phys. Lett.* **73**(20), 2926–2928 (1998).
- ⁷R. García, *Chem. Soc. Rev.* **49**(16), 5850–5884 (2020).
- ⁸S. Santos, K. Gadelrab, C.-Y. Lai, T. Olukan, J. Font, V. Barcons, A. Verdaguer, and M. Chiesa, *J. Appl. Phys.* **129**(13), 134302 (2021).
- ⁹J. R. Lozano and R. García, *Phys. Rev. Lett.* **100**, 076102–076105 (2008).
- ¹⁰F. J. Giessibl, *Rev. Mod. Phys.* **75**(3), 949 (2003).
- ¹¹S. Benaglia, C. A. Amo, and R. García, *Nanoscale* **11**(32), 15289–15297 (2019).
- ¹²E. T. Herruzo, A. P. Perrino, and R. García, *Nat. Commun.* **5**(1), 3126 (2014).
- ¹³V. G. Gisbert, S. Benaglia, M. R. Uhlig, R. Proksch, and R. García, *ACS Nano* **15**(1), 1850–1857 (2021).
- ¹⁴B. Rajabifar, A. Bajaj, R. Reifenberger, R. Proksch, and A. Raman, *Nanoscale* **13**(41), 17428–17441 (2021).
- ¹⁵S. D. Solares, *Beilstein J. Nanotechnol.* **5**, 1649–1663 (2014).
- ¹⁶C.-Y. Lai, S. Perri, S. Santos, R. García, and M. Chiesa, *Nanoscale* **8**(18), 9688–9694 (2016).
- ¹⁷C.-Y. Lai, S. Santos, and M. Chiesa, *ACS Nano* **10**(6), 6265–6272 (2016).
- ¹⁸M. Kocun, A. Labuda, W. Meinhold, I. Revenko, and R. Proksch, *ACS Nano* **11**(10), 10097–10105 (2017).
- ¹⁹S. Santos, C.-Y. Lai, T. Olukan, and M. Chiesa, *Nanoscale* **9**(16), 5038–5043 (2017).
- ²⁰V. G. Gisbert and R. García, *ACS Nano* **15**(12), 20574–20581 (2021).
- ²¹H. C. Hamaker, *Physica* **4**(10), 1058–1072 (1937).
- ²²J. N. Israelachvili, *Intermolecular and Surface Forces* (Elsevier Academic Press, London, 2005).
- ²³C.-Y. Lai, T. Olukan, S. Santos, A. Al Ghaferi, and M. Chiesa, *Chem. Commun. (Camb.)* **51**(99), 17619–17622 (2015).
- ²⁴J. Colchero, A. Gil, and A. M. Baró, *Phys. Rev. B* **64**(24), 245403 (2001).
- ²⁵H. Goldstein, C. Poole, and J. L. Safko, *Classical Mechanics* (Pearson, 2001).
- ²⁶N. Oinonen, C. Xu, B. Alldritt, F. F. Canova, F. Urtev, S. Cai, O. Krejčí, J. Kannala, P. Liljeroth, and A. S. Foster, *ACS Nano* **16**(1), 89–97 (2022).
- ²⁷A. Klaassen, F. Liu, F. Mugele, and I. Siretanu, *Langmuir* **38**(3), 914–926 (2022).
- ²⁸M. Lv, X. Sun, Y. Chen, T. Taniguchi, K. Watanabe, M. Wu, J. Wang, and J. Xue, *Adv. Mater.* **34**(51), 2203990 (2022).
- ²⁹S. He, M. Guo, Y. Wang, Y. Liang, and Y. Shen, *Adv. Mater.* **34**(24), 2202181 (2022).
- ³⁰D. V. Karpinsky, O. M. Fesenko, M. V. Silibin, S. V. Dubkov, M. Chaika, A. Yaremkevich, A. Lukowiak, Y. Gerasymchuk, W. Stręk, A. Pakalniškis, R. Skaudzius, A. Kareiva, Y. M. Fomichov, V. V. Shvartsman, S. V. Kalinin, N. V. Morozovskiy, and A. N. Morozovska, *Sci. Rep.* **9**(1), 10417 (2019).
- ³¹D. Passeri, L. Angeloni, and M. Rossi, in *New Trends in Nanoparticle Magnetism*, edited by D. Peddis, S. Laureti, and D. Fiorani (Springer International Publishing, Cham, 2021), pp. 285–300.
- ³²V. G. Gisbert, C. A. Amo, M. Jaafar, A. Asenjo, and R. García, *Nanoscale* **13**(3), 2026–2033 (2021).
- ³³J. W. Li, J. P. Cleveland, and R. Proksch, *Appl. Phys. Lett.* **94**(16), 163118 (2009).
- ³⁴R. Steidel, *An Introduction to Mechanical Vibrations*, 3rd ed. (John Wiley & Sons, 1989).
- ³⁵M. Sands, R. Feynman, and R. Leighton, *The Feynman Lectures on Physics* (Basic Books, 2011).
- ³⁶D. Gregory, *Classical Mechanics* (Cambridge University Press, 2006).
- ³⁷C. Amo, *Microscopía de Fuerza Bimodal y no Resonante para Medir Propiedades Físicas y Químicas a Escala Nanométrica* (Universidad Autónoma de Madrid, 2019).
- ³⁸R. García, C. J. Gómez, N. F. Martínez, S. Patil, C. Dietz, and R. Magerle, *Phys. Rev. Lett.* **97**, 016103–016104 (2006).
- ³⁹R. García and A. San Paulo, *Phys. Rev. B* **60**(7), 4961 (1999).
- ⁴⁰J. Israelachvili, *Intermolecular & Surface Forces*, 2nd ed. (Academic Press, 1991).
- ⁴¹S. Hu and A. Raman, *Nanotechnology* **19**(37), 375704 (2008).
- ⁴²M. D. Aksoy and A. Atalar, *Phys. Rev. B* **83**(7), 075416 (2011).
- ⁴³E. T. Herruzo and R. García, *Beilstein J. Nanotechnol.* **3**, 198–206 (2012).
- ⁴⁴S. Kawai, T. Glatzel, S. Koch, B. Such, A. Baratoff, and E. Meyer, *Phys. Rev. Lett.* **103**, 220801–220804 (2009).